nature materials

ARTICLES

https://doi.org/10.1038/s41563-018-0084-7

An autonomously electrically self-healing liquid metal–elastomer composite for robust soft-matter robotics and electronics

Eric J. Markvicka[1,2,5], Michael D. Bartlett[3,5], Xiaonan Huang[1,4] and Carmel Majidi[1,2,4]*

Large-area stretchable electronics are critical for progress in wearable computing, soft robotics and inflatable structures. Recent efforts have focused on engineering electronics from soft materials—elastomers, polyelectrolyte gels and liquid metal. While these materials enable elastic compliance and deformability, they are vulnerable to tearing, puncture and other mechanical damage modes that cause electrical failure. Here, we introduce a material architecture for soft and highly deformable circuit interconnects that are electromechanically stable under typical loading conditions, while exhibiting uncompromising resilience to mechanical damage. The material is composed of liquid metal droplets suspended in a soft elastomer; when damaged, the droplets rupture to form new connections with neighbours and re-route electrical signals without interruption. Since self-healing occurs spontaneously, these materials do not require manual repair or external heat. We demonstrate this unprecedented electronic robustness in a self-repairing digital counter and self-healing soft robotic quadruped that continue to function after significant damage.

Traditional electronics are typically composed of intrinsically rigid and brittle materials that have limited deformability or resistance to bending, stretching and impact loading. Efforts to create soft and deformable circuits have largely focused on soft conductive polymers[1,2], serpentine and wavy circuit interconnects[3–5], and the integration of conductive fluids into gels[6,7] and soft microfluidic channels[8–10]. These advances have resulted in highly flexible, stretchable and conformable electronics that function as artificial skin and nervous tissue in a broad range of emerging applications, from 'second-skin' wearable computing[11–13] to bio-inspired soft robotics[14,15]. However, the soft elastic materials typically used for these circuits and applications are susceptible to tearing, puncturing and other forms of mechanical failure that lead to loss in electrical conductivity. This limitation greatly prohibits the use of soft electronics in applications such as remote teleoperation or autonomous field robotics where repair is challenging or impossible. While rigid substrates and packaging can be used to mitigate damaging stress concentrations in traditional electronics, such encapsulation will interfere with the elasticity of soft circuits. Instead, further advancements in these emerging fields depend on new classes of soft electronic materials that, like natural skin or nervous tissue, are self-healing and remain functional even as material is torn, ruptured or removed.

In recent years, there has been exciting progress in the development of soft electronics that are capable of self-healing or that can be repaired when damaged to restore electrical functionality. These include semiconducting polymers[16], conductive polymer networks[17–19], ionic hydrogels[20], liquid metal (LM) microcapsules patterned on gold lines[21] and LM microfluidics[22,23]. Although promising, these existing methods have at least one of several limitations: extended period of functional loss during self-repair; need for manual reassembly; dependency on external or redundant electronics for damage detection and circuit restoration; need for external energy sources such as heat, light or mechanical energy; or dependency on non-ambient conditions such as increased relative humidity or temperature. Overcoming these limitations has the potential to dramatically improve the longevity, performance and functionality of deformable electronic materials.

Here, we introduce a material architecture and framework for creating circuit interconnects that are capable of autonomous, electrical self-healing. The soft and highly deformable material is composed of droplets of Ga-based LM alloy (gallium–indium, eutectic; EGaIn) embedded in a soft, silicone elastomer. In its natural (original) state following synthesis, this composite is electrically insulating, even for high LM volume fractions ($\phi \geq 50\%$). However, application of extreme local pressure causes the LM droplets to rupture and coalesce to form locally conductive pathways with high electrical conductivity ($\sigma = 1.37 \times 10^3\,\mathrm{S\,cm^{-1}}$ for $\phi = 50\%$; Fig. 1a,b and Supplementary Movie 1). This mechanically controlled response enables circuits to be both created and subsequently reconfigured when damage is induced, through the autonomous, in situ formation of new electrical pathways. This self-repairing property is demonstrated in Fig. 1c, which shows how a four-channel serial clock display continues to operate as the power, data and clock lines undergo extreme mechanical damage, including cutting, tearing and the complete removal of material (Supplementary Movie 2). This extraordinary resilience is possible through the mechanism illustrated in Fig. 1b, which shows how damage induces the formation of new droplet–droplet connections that re-route the electrical conductor around the damaged region.

Previous LM–elastomer systems have focused on microfluidic circuits and LM embedded elastomers (LMEEs) through dispersions of LM droplets, drop-casted LM films or backfilled cellular structures[22–33]. For the case of microfluidic circuits, self-healing has been demonstrated but conductivity is temporarily lost and may require manual intervention to restore function[22,23]. Previous

[1]Integrated Soft Materials Lab, Carnegie Mellon University, Pittsburgh, PA, USA. [2]Robotics Institute, Carnegie Mellon University, Pittsburgh, PA, USA. [3]Material Science & Engineering, Iowa State University, Ames, IA, USA. [4]Mechanical Engineering, Carnegie Mellon University, Pittsburgh, PA, USA. [5]These authors contributed equally: Eric J. Markvicka, Michael D. Bartlett. *e-mail: cmajidi@andrew.cmu.edu

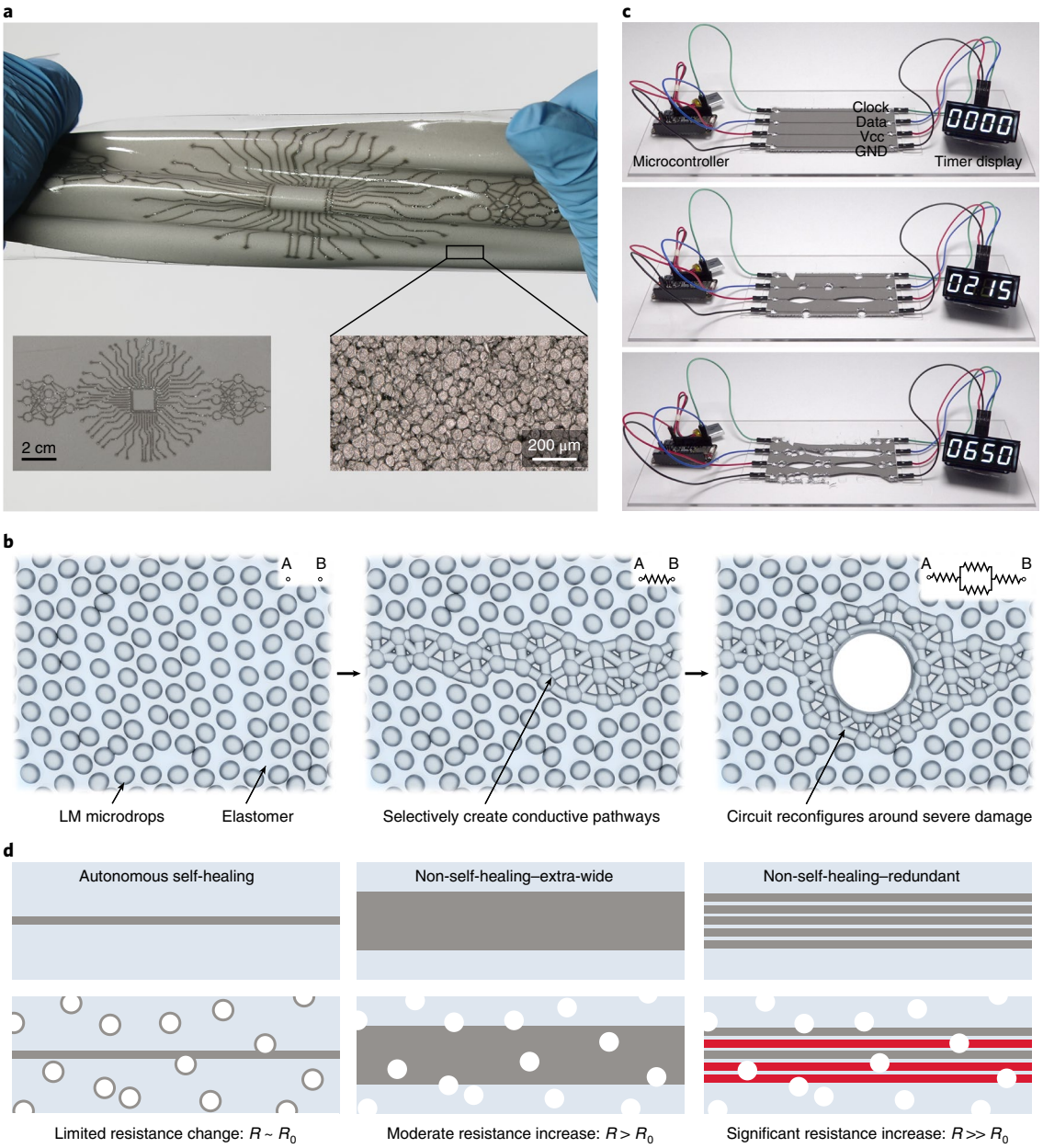

Fig. 1 | Self-healing soft matter composite. a, A LM-elastomer composite being stretched and twisted with an intricate design of electrically conductive traces. The lower left inset shows the undeformed sample and lower right inset is an optical micrograph showing the LM microdroplets in the elastomer at $\phi = 50\%$. **b**, A schematic illustration of the self-healing mechanism where an initially insulating composite is selectively compressed to create electrically conductive LM traces. Following damage, the LM trace autonomously reconfigures and maintains electrical conductivity. Inset: equivalent electrical circuit schematic. **c**, Example of the reconfigurable material ($\phi = 50\%$) transmitting d.c. power (Vcc, positive supply voltage; GND, ground) and digital communication signals to operate a counter display. As severe damage is induced, the counter maintains operation, which requires all four traces to constantly maintain electrical conductivity. **d**, A schematic diagram of different damage mitigation strategies. From left to right: the new autonomous self-healing damage mitigation strategy presented here; a non-self-healing trace that is significantly wider than the expected damage size to prevent failure; redundant non-self-healing traces to reduce the probability of failure.

efforts in LMEE synthesis[24–27,30–32,34] resulted in material compositions and microstructures that achieved electrical conductivity only at very high volume loadings $\phi \geq 50\%$ (if at all) and did not exhibit autonomous self-repair. In addition, light pressure (<100 kPa) could form conductive networks by 'mechanically sintering' LM nanoparticle films, and general handling may lead to unintended activation between neighbouring traces, resulting in electrical failure[25]. Although not soft or stretchable, autonomous self-healing had been previously demonstrated using LM droplets embedded in rigid materials ($E > 2.8$ GPa); however, conductivity is initially interrupted after damage and self-healing was limited to a single event as the LM is depleted during healing[21].

By combining recent work on LM, fluidic self-healing and mechanical sintering, we are able to demonstrate a soft, stretchable circuit that is electrically stable under typical operational loading conditions but capable of instantaneous electrical self-healing under multiple, extreme damage events. In contrast to previous work, the material composition and LM microstructure presented

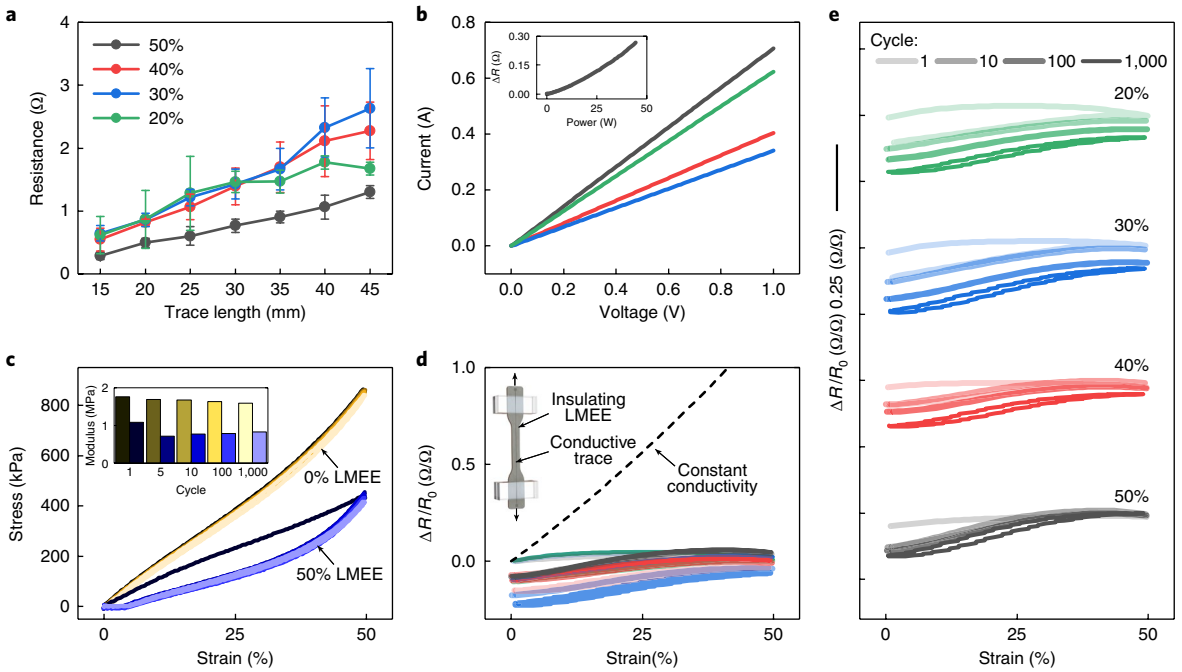

Fig. 2 | Electrical and mechanical characterization. a, Resistance as a function of trace length for four different volume loadings ($\phi = 50$, 40, 30, 20%). The error bars are the standard deviation for $N = 3$ samples. **b**, Current–voltage curves up to 1 V for a 45 mm trace ($\phi = 50$, 40, 30, 20%) and (inset) absolute change in resistance as a function of applied power as 5 A is sourced to the $\phi = 50$% sample; refer to the legend in **a**. **c**, Stress versus strain under uniaxial cyclic loading to 50% strain for $\phi = 0$% and $\phi = 50$%, up to 1,000 cycles. Inset: modulus as a function of loading cycle. **d**, Normalized resistance as a function of strain ($\phi = 50$, 40, 30, 20%) and theoretical prediction using Ohm's law for an incompressible solid with fixed volumetric resistivity; refer to the legend in **a** for volume loading and **e** for cycle. **e**, Normalized resistance as a function of strain ($\phi = 50$, 40, 30, 20%); note, the *y* axis offset is applied to each volume loading to assist in visualization of the data.

here is naturally robust to inadvertent activation that could lead to electrical shorting. Since the LM droplets are dispersed in an elastomeric phase instead of a continuous particle film, significant stress shielding is provided that protects the circuit from unintended activation. Furthermore, by exhibiting an autonomous and instantaneous response, our electrical wiring is uniquely capable of continuous functionality when subject to the sparse and localized but spatially random damage that frequently occurs in real-world applications. When compared to non-self-healing circuits with redundant or extra-wide traces, this self-healing architecture provides circuit interconnects that have a smaller footprint, which are statistically less likely to be damaged, and exhibit a limited drop in electrical conductivity even when damage has occurred (Fig. 1d). Furthermore, the addition of a thin elastomer sealing layer after fabrication or selective patterning (Supplementary Fig. 1 and Supplementary Movie 3) can be used to protect the underlying circuit and help alleviate unintended activation between neighbouring traces.

LM–elastomer composite

The self-healing material is composed of EGaIn microdroplets (75% Ga, 25% In by weight; Solution Materials, LLC) dispersed in a soft silicone elastomer (Sylgard 184; Dow Corning). EGaIn is selected as the liquid filler due to the combination of high electrical conductivity, low viscosity and non-toxic characteristics[35,36]. The composite is fabricated by mechanically mixing a range of LM loadings from $\phi = 20$ to 50% with uncured elastomer, creating a dispersion of generally ellipsoidal particles on the order of 50 µm (Supplementary Fig. 2 and see Methods). After initial fabrication, the solid–liquid hybrid composite is electrically insulating due to a lack of percolating networks and the presence of an insulating oxide skin that develops on the surface of the LM droplets.

Trace patterning. Application of local pressure induces the formation of conductive pathways, which are created as LM droplets rupture to form percolated networks. These pathways are internal to the composite and can function as traces for power and data transmission within elastomer-embedded soft circuits. Since the remaining material is unaffected, multiple traces can be constructed that are electrically insulated from each other. To create a patterned circuit, we utilize a *X*–*Y* pen plotter (Explore, Cricut) that enables intricate circuit designs to be digitally created and implemented rapidly in a maskless fabrication approach (Supplementary Movie 1 and see Methods). For the current approach, circuit designs require a 2.5 mm centre-to-centre spacing to prevent unintended shorting between adjacent, 500-µm-wide traces (see Supplementary Note 1, Methods and Supplementary Fig. 3).

Electromechanical characterization. The electrical resistance as a function of trace length was characterized for LM volume loadings of $\phi = 20$ to 50%. The $\phi = 50$% sample exhibits the highest electrical conductivity ($\sigma = 1.37 \times 10^3$ S cm^{-1}) across this range and maintains a constant conductivity (assuming a constant cross-sectional area) making it useful for various functions within electronic circuits (Fig. 2a). The voltage across a conductive trace was then monitored as current was sourced. The material exhibits a linear *I*–*V* response (constant resistance) up to 1 V for all volume loadings of LM (Fig. 2b), and is in good agreement with Fig. 2a ($\ell = 45$ mm). As the applied power is increased (up to 5 A), Fig. 2b inset shows a small increase in absolute resistance as a function of applied power for a $\phi = 50$% sample. This deviation in absolute resistance is likely to be due to the decrease in volumetric conductivity as the local temperature of the LM increases due to Joule heating, corresponding to a relative change of 44 °C (see Methods).

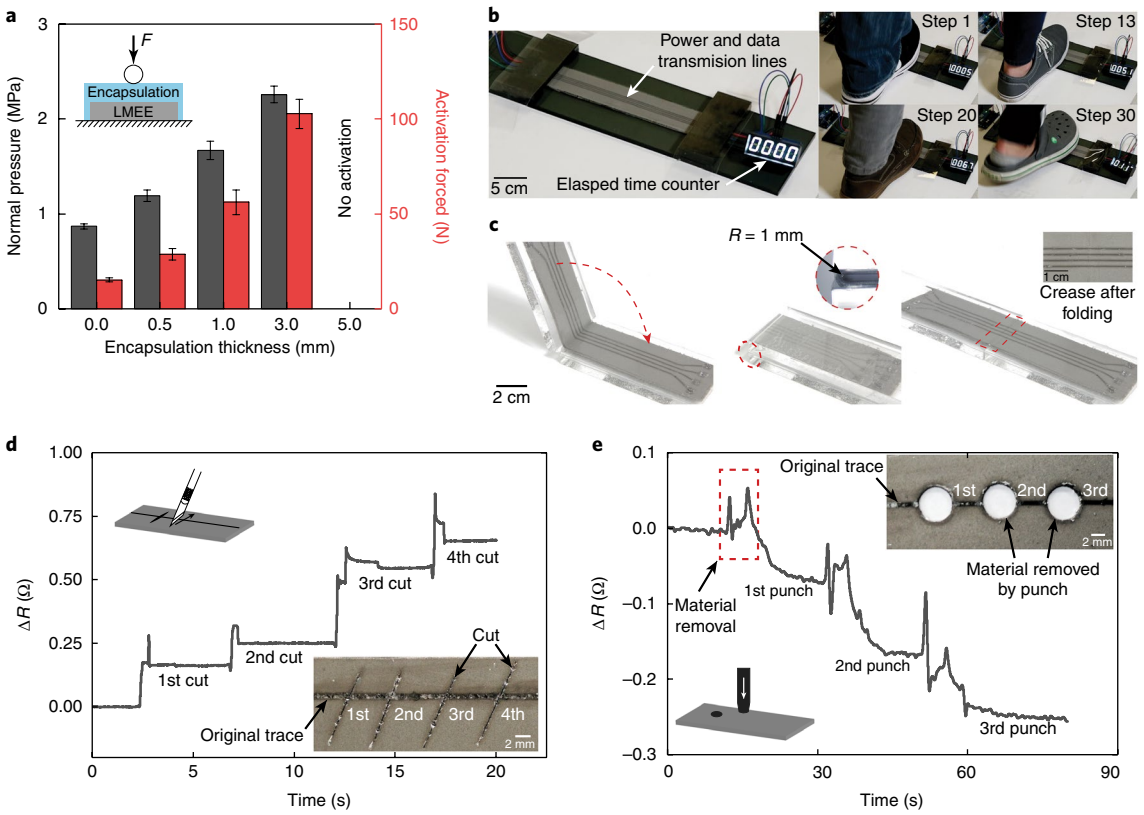

Fig. 3 | Autonomous self-healing response ($\phi = 50\%$). a, Critical activation pressure/force required to induce unintentional activation of closely neighbouring traces (5 mm trace spacing) for different encapsulation thicknesses ($t = 0$, 0.5, 1, 3 and 5 mm). The error bars correspond to the standard deviation ($N = 5$). **b**, The robust nature of the material to everyday loading is demonstrated by walking across the traces of a digital clock in various types of footwear without any unintended activation. **c**, Closely neighbouring traces (2.5 mm trace spacing) are electrically stable under folding up to 180° with a bend radius of 1 mm. **d**,**e**, Resistance as a function of time for high-aspect-ratio damage from a razor blade (**d**) and low-aspect-ratio damage from a hole punch (**e**). Depending on the aspect ratio of the damage, the resistance of the trace can increase or decrease. During damage, the circuit is autonomously reconfigured without intervention or loss of conductivity.

The LM–elastomer composite is shown to be soft (elastic modulus ≃0.8 MPa) and exhibit low hysteresis elasticity after the first loading cycle when loaded up to 50% strain for 1,000 loading cycles (Fig. 2c). Extended cyclical loading was performed for 1 million cycles up to 40% tensile strain, which is below the strain limit of the composite. Before mechanical failure, there is no loss in electrical conductivity (Supplementary Fig. 4). As shown in Supplementary Fig. 5, the trace exhibits little change in electrical resistance over the course of the 1 million loading cycles.

Electro-mechanical coupling is examined by measuring the electrical resistance as a function of uniaxial strain (see Methods). Each volume loading is cycled to 50% strain for 1,000 loading cycles. As shown in Fig. 2e, a small increase in normalized resistance is evident in the initial extension for the first loading cycle for all volume loadings. However, when returning to the undeformed length, the resistance decreases below the original, undeformed value for all samples. On subsequent loadings, the 50% sample exhibits a stable response for 1,000 loading cycles, while the 20–40% samples actually show a reduction in normalized resistance. In all cases, following stretching to 50% strain the maximum increase in resistance is less than 10% (Fig. 2d). We hypothesize that when the material is strained, the LM within the droplets flows into the connecting pathways between droplets, reducing the electro-mechanical coupling effects. This behaviour contrasts sharply with traditional incompressible, stretchable conductors, where the normalized trace resistance ($\Delta R/R_0$) should increase as $\lambda^2 - 1$, or 1.25× at 50% strain, where stretch (λ) is defined as the ratio of the final length and the initial length ($\lambda = L/L_0$)[37]. Such a characteristic increase in circuit resistance is undesirable for most circuit applications, where even more extreme increases are observed in soft-matter systems that utilize conductive particle-filled elastomers and soft co-polymer blends. These results show the robust and reliable nature of the self-healing composite, displaying high electrical conductivity and mechanically robust functionality over repeated loading cycles.

Material encapsulation. To provide further protection from non-damaging, environmental conditions (for example, contact pressure, shear forces and folding), the composite can be encapsulated within an elastomer sealing layer to help prevent or completely eliminate ($t \geq 5$ mm) further trace formation that results in undesired activation between closely neighbouring traces (Fig. 3a). To experimentally characterize the electrical stability of the device under contact pressure, a glass cylindrical indenter was positioned across two closely neighbouring traces and pressed into the composite ($\phi = 50\%$, $t = 500\,\mu$m) until undesired activation occurred (see Methods). The thickness of the self-healing composite has a negligible influence on the activation pressure (Supplementary Fig. 6). Furthermore, the composite is capable of withstanding repeated compressive loads to 35 N ($p_{max} = 1.32$ MPa) for 1,000 loading cycles without unintended activation occurring for a $\phi = 50\%$ sample with a 1 mm encapsulation layer (see Supplementary Information). Conversely, the highest localized pressure under the foot during walking of young adults is ~0.33 MPa (ref. [38]). This indicates that

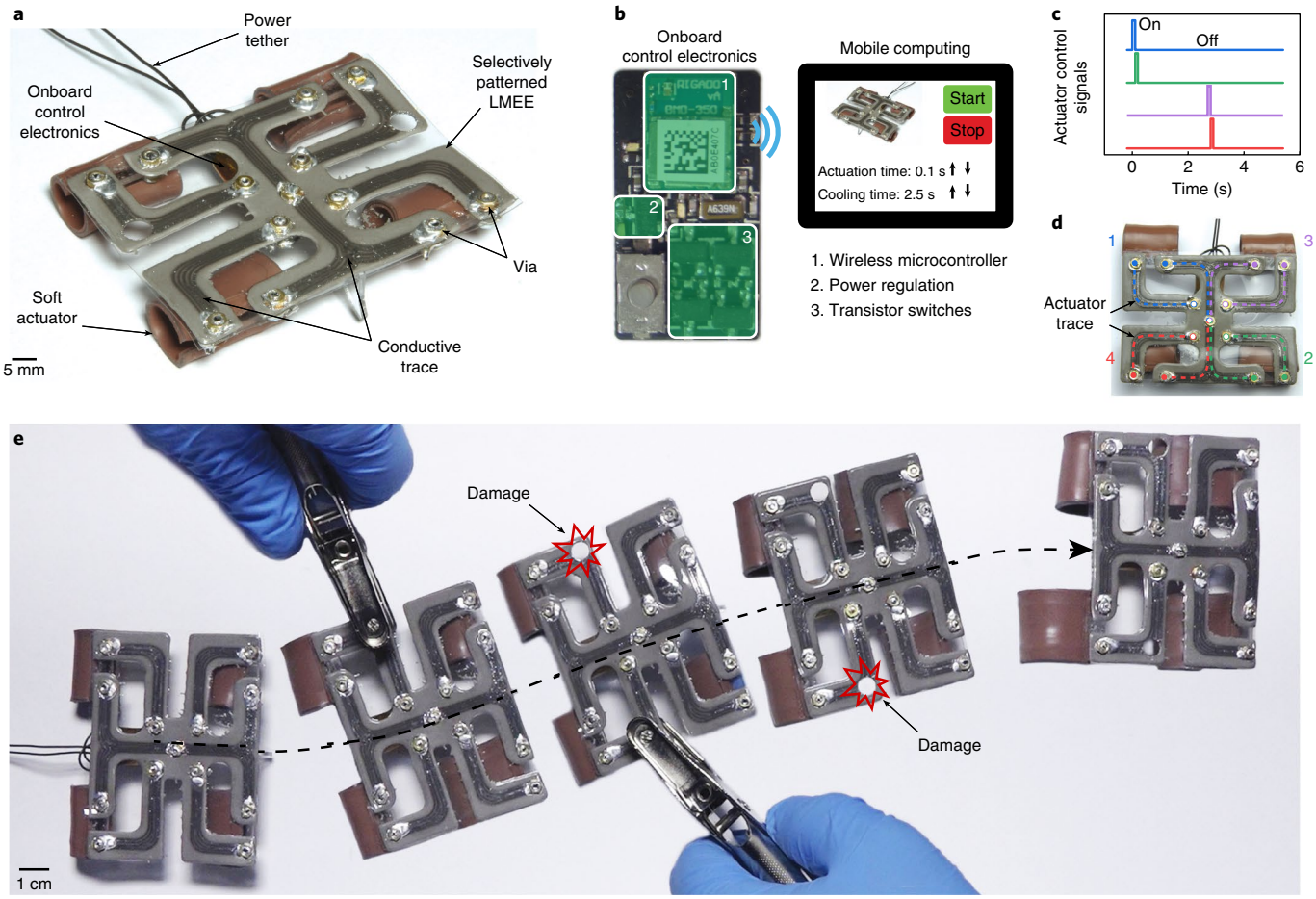

Fig. 4 | Autonomously self-healing soft robot ($\phi = 50\%$). a, A soft quadruped with autonomously self-healing soft-matter electronics. **b**, The robot is controlled using a mobile computing platform that wirelessly transmits high- and low-level commands to onboard control electronics. **c**, Actuation sequence for the soft quadruped. **d**, Schematic of high-power signal routing, connecting the onboard control electronics (white-filled circles) to the soft actuators (colour-filled circles); the trace is colour-coded with reference to **c**. **e**, Movie frame sequence from the top-down view (Supplementary Movie 5) of the soft robot traversing smooth terrain. The robot encounters puncture damage from a hole punch and the electrical pathway is autonomously reconfigured around the damaged region without loss of electrical conductivity. There is no apparent change in the gait of the soft robot after damage, as the robot continues traversing the smooth terrain as before without manual intervention, use of external energy sources or redundant electronics.

walking pressure would not be sufficient to activate the composite in the most vulnerable situation. As experimentally demonstrated with a thin elastomer sealing layer ($t = 1$ mm), the self-healing circuit ($\phi = 50\%$, 2.5 mm trace spacing) is capable of undergoing normal walking conditions for 31 steps with 10 footwear variations without any unintended shorting between traces for a digital clock (Fig. 3b and Supplementary Movie 4).

To further investigate unintended trace formation from non-damaging surface tractions, the device was experimentally characterized using a single-lap shear joint (Supplementary Fig. 7). The device remained electrically stable without an encapsulation layer under a maximum shear stress of ~0.24 MPa. The device can also endure surface abrasion when encapsulated with a thin elastomer sealing layer ($t = 1$ mm; Supplementary Fig. 8). Further quantitative shear stress experiments were performed, where a tangential shear force was applied to a spherical indenter that is pressed into the composite. The indenter is sheared across two closely neighbouring traces until undesired activation occurred (see Supplementary Information). The device is approximately twice as resilient to the maximum normal pressure under tangential shear when sealed with a thin elastomer layer ($P = 0.75$ MPa, $t = 1$ mm; Supplementary Fig. 9). In addition, we find that the device is electrically stable up to a bend radius of 1 mm (1.25× the overall thickness), which is comparable to flexible circuits that have a minimum bend radius of 6× to 12× the overall thickness (for 0.1-mm-thick flexible circuit, $R = 0.6$ to 1.2 mm; Fig. 3c). Lastly, extended cyclic loading was performed to 40% strain for 1 million loading cycles, where no unintended activation occurred between two closely neighbouring traces (Supplementary Fig. 5). These results demonstrate that the device is capable of withstanding general handling and the rigours of daily use, where, in practice, conductive networks are formed only under extreme loading conditions associated with tearing, puncturing and material removal.

Damage response. As demonstrated in Fig. 1, the composite material is capable of being severely damaged while maintaining electrical conductivity. The self-healing response of the material is further investigated with controlled cutting and puncturing experiments. Here, we measure the resistance of a trace while mechanical damage is inflicted. First, linear cuts with a razor blade are investigated. As shown in Fig. 3d, a minimal increase in absolute resistance ($<1\,\Omega$) is observed with subsequent cuts; furthermore, the material continuously maintains electrical conductivity during and after damage has occurred. As the composite is punctured, the LM droplets on the damaged surface are ruptured and a stabilizing oxide layer is formed when the gallium-based LM is exposed to oxygen,

preventing unwanted flow of LM[39]. Next, a series of circular holes with perimeter P are created along the length of the trace (Fig. 3e). Remarkably, the resistance is observed to decrease as subsequent holes are created. This counterintuitive response is due to the electrical reconfiguration of the damaged circuit (Fig. 1b). When a piece of material with trace length L_t is removed from the circuit, the original trace is replaced by two traces of length $\alpha\pi L_t$ and $(1-\alpha)\pi L_t$, where $0<\alpha<1$ is the ratio of the perimeter on one side of the trace. If we assume constant resistivity and $\alpha P(1-\alpha)<L_t$, the overall resistance of the circuit will be reduced, where maximum reduction occurs when the length of the perimeter is symmetric about the trace ($\alpha=0.5$). This model also predicts a rise in resistance for high-aspect-ratio damage, which is observed for the linear cuts in Fig. 3e (see Supplementary Information).

Soft robotics demonstration

This electronically self-healing material is particularly enabling for wearable electronics, soft robotics and inflatable technologies when combined with advanced integrated circuits. To demonstrate the capabilities of the self-healing material for demanding applications, we produce a soft robotic quadruped with autonomously self-healing electrical wiring to route the power signals from the onboard control electronics to the soft actuators (Fig. 4a). While not shown here, mechanical (structural) self-healing has previously been demonstrated in pneumatic robotic grippers[40,41]. The soft actuators used here are composed of shape memory alloy (SMA) wires embedded in thermal tape and are sequentially actuated (Fig. 4c,d) through direct Joule heating to enable robot locomotion (see Methods). The soft robot is powered using a lightweight tether and is wirelessly controlled from a mobile computing platform (Fig. 4b, see Supplementary Information). Figure 4e shows that the resulting quadruped is capable of traversing smooth terrain and is resilient to puncture damage with no apparent change in the gait of the soft quadruped. Remarkably, the robot is able to continue traversing the smooth terrain as before without manual intervention, use of external energy sources, redundant electronics or changes to the environmental conditions (Supplementary Movie 5). This is especially surprising since over 50% of the width of the power trace is removed when damaged and any drastic changes in the resistance (~5 Ω) of the circuit wiring would prevent the limb from continuing its powered actuation due to local heating of the damaged region instead of the thermal actuator. This implementation highlights the versatility of the autonomously self-healing soft-matter composite, the ease of integration with complex systems and the ability to handle high currents for high-power/energy-demanding applications even when damage occurs.

Outlook

We have introduced a soft-matter composite for mechanically robust, electrically self-healing circuit interconnects for power and data transmission that instantaneously repairs itself under extreme mechanical damage. Circuits produced with conductive traces of this material remain fully and continuously operational even when the traces are severed, torn, or punctured or material is removed. Furthermore, if not initially activated, the composite remains electrically insulating under non-damaging environmental conditions when sealed with a thin elastomer layer. This unprecedented level of robust functionality has the potential to enable soft-matter electronics and machines to exhibit the extraordinary resilience of soft biological tissue and organisms. In addition to the self-healing response, this material exhibits a high electrical conductivity that does not change with stretch and is ideally suited for stretchable electronics with strain-invariant circuit properties. Moreover, it is uniquely suited as 0.01–0.1-m-scale wiring (for example, power, data and clock lines) for applications where the damaged regions are small and sparse but randomly distributed over a large area. The circuit achieves 'effective redundancy' or 'widening' in an autonomous manner and only in locations where damage occurs (Fig. 1d). Such responses correspond to a limited change in overall conductivity of the electrical conductor. This continuous and stable electrical conductivity is especially critical for power transmission but can also be important for certain types of data transmission. Lastly, the relatively simple and versatile circuit patterning approach allows for implementation in diverse applications. Nonetheless, development in the precise control of particle size, arrangement, use of surfactants to modify oxide layer properties, and composition could potentially allow for additional capabilities, such as transparency and electrical or mechanical tunability.

Methods

Methods, including statements of data availability and any associated accession codes and references, are available at https://doi.org/10.1038/s41563-018-0084-7.

Received: 22 January 2018; Accepted: 18 April 2018;
Published online: 21 May 2018

References

1. Wang, Y. et al. A highly stretchable, transparent, and conductive polymer. *Sci. Adv.* **3**, e1602076 (2017).
2. Bartlett, M. D., Markvicka, E. J. & Majidi, C. Rapid fabrication of soft, multilayered electronics for wearable biomonitoring. *Adv. Funct. Mater.* **26**, 8496–8504 (2016).
3. Kim, D.-H. et al. Epidermal electronics. *Science* **333**, 838–843 (2011).
4. Someya, T. et al. Conformable, flexible, large-area networks of pressure and thermal sensors with organic transistor active matrixes. *Proc. Natl Acad. Sci. USA* **102**, 12321–12325 (2005).
5. Sun, Y., Choi, W. M., Jiang, H., Huang, Y. Y. & Rogers, J. A. Controlled buckling of semiconductor nanoribbons for stretchable electronics. *Nat. Nanotechnol.* **1**, 201–207 (2006).
6. Keplinger, C. et al. Stretchable, transparent, ionic conductors. *Science* **341**, 984–987 (2013).
7. Kim, C.-C., Lee, H.-H., Oh, K. H. & Sun, J.-Y. Highly stretchable, transparent ionic touch panel. *Science* **353**, 682–687 (2016).
8. Chossat, J.-B., Park, Y.-L., Wood, R. J. & Duchaine, V. A soft strain sensor based on ionic and metal liquids. *IEEE Sens. J.* **13**, 3405–3414 (2013).
9. Frutiger, A. et al. Capacitive soft strain sensors via multicore–shell fiber printing. *Adv. Mater.* **27**, 2440–2446 (2015).
10. Dickey, M. D. Stretchable and soft electronics using liquid metals. *Adv. Mater.* **29**, 1606425 (2017).
11. Hammock, M. L., Chortos, A., Tee, B. C.-K., Tok, J. B.-H. & Bao, Z. 25th anniversary article: the evolution of electronic skin (e-skin): a brief history, design considerations, and recent progress. *Adv. Mater.* **25**, 5997–6038 (2013).
12. Amjadi, M., Kyung, K.-U., Park, I. & Sitti, M. Stretchable, skin-mountable, and wearable strain sensors and their potential applications: A review. *Adv. Funct. Mater.* **26**, 1678–1698 (2016).
13. Chortos, A., Liu, J. & Bao, Z. Pursuing prosthetic electronic skin. *Nat. Mater.* **15**, 937–950 (2016).
14. Rus, D. & Tolley, M. T. Design, fabrication and control of soft robots. *Nature* **521**, 467–475 (2015).
15. Rich, S., Wood, R. J. & Majidi, C. Untethered soft robotics. *Nat. Electron.* **1**, 102–112 (2018).
16. Oh, J. Y. et al. Intrinsically stretchable and healable semiconducting polymer for organic transistors. *Nature* **539**, 411–415 (2016).
17. Tee, B. C., Wang, C., Allen, R. & Bao, Z. An electrically and mechanically self-healing composite with pressure-and flexion-sensitive properties for electronic skin applications. *Nat. Nanotechnol.* **7**, 825–832 (2012).
18. Williams, K. A., Boydston, A. J. & Bielawski, C. W. Towards electrically conductive, self-healing materials. *J. R. Soc. Interface* **4**, 359–362 (2007).
19. Zhang, S. & Cicoira, F. Water-enabled healing of conducting polymer films. *Adv. Mater.* **29**, 1703098 (2017).
20. Cao, Y. et al. A transparent, self-healing, highly stretchable ionic conductor. *Adv. Mater.* **29**, 1605099 (2017).
21. Blaiszik, B. J. et al. Autonomic restoration of electrical conductivity. *Adv. Mater.* **24**, 398–401 (2012).
22. Palleau, E., Reece, S., Desai, S. C., Smith, M. E. & Dickey, M. D. Self-healing stretchable wires for reconfigurable circuit wiring and 3D microfluidics. *Adv. Mater.* **25**, 1589–1592 (2013).
23. Li, G., Wu, X. & Lee, D.-W. A galinstan-based inkjet printing system for highly stretchable electronics with self-healing capability. *Lab Chip* **16**, 1366–1373 (2016).

24. Boley, J. W., White, E. L. & Kramer, R. K. Mechanically sintered gallium-indium nanoparticles. *Adv. Mater.* **27**, 2355–2360 (2015).
25. Mohammed, M. G. & Kramer, R. All-printed flexible and stretchable electronics. *Adv. Mater.* **29**, 1604965 (2017).
26. Lin, Y. et al. Handwritten, soft circuit boards and antennas using liquid metal nanoparticles. *Small* **11**, 6397–6403 (2015).
27. Fassler, A. & Majidi, C. Liquid-phase metal inclusions for a conductive polymer composite. *Adv. Mater.* **27**, 1928–1932 (2015).
28. Bartlett, M. D. et al. High thermal conductivity in soft elastomers with elongated liquid metal inclusions. *Proc. Natl Acad. Sci. USA* **114**, 2143–2148 (2017).
29. Park, J. et al. Three-dimensional nanonetworks for giant stretchability in dielectrics and conductors. *Nat. Commun.* **3**, 916 (2012).
30. Van Meerbeek, I. M. et al. Morphing metal and elastomer bicontinuous foams for reversible stiffness, shape memory, and self-healing soft machines. *Adv. Mater.* **28**, 2801–2806 (2016).
31. Bartlett, M. D. et al. Stretchable, high-*k* dielectric elastomers through liquid-metal inclusions. *Adv. Mater.* **28**, 3726–3731 (2016).
32. Liang, S. et al. Liquid metal sponges for mechanically durable, all-soft, electrical conductors. *J. Mater. Chem. C* **5**, 1586–1590 (2017).
33. Wang, J. et al. Printable superelastic conductors with extreme stretchability and robust cycling endurance enabled by liquid metal particles. *Adv. Mater.* **30**, 1706157 (2018).
34. Jeong, S. H. et al. Mechanically stretchable and electrically insulating thermal elastomer composite by liquid alloy droplet embedment. *Sci. Rep.* **5**, 18257 (2015).
35. Dickey, M. D. et al. Eutectic gallium-indium (EGaIn): a liquid metal alloy for the formation of stable structures in microchannels at room temperature. *Adv. Funct. Mater.* **18**, 1097–1104 (2008).
36. Chiechi, R. C., Weiss, E. A., Dickey, M. D. & Whitesides, G. M. Eutectic gallium-indium (EGaIn): A moldable liquid metal for electrical characterization of self-assembled monolayers. *Angew. Chem.* **120**, 148–150 (2008).
37. Kim, H.-J., Son, C. & Ziaie, B. A multiaxial stretchable interconnect using liquid-alloy-filled elastomeric microchannels. *Appl. Phys. Lett.* **92**, 011904 (2008).
38. Hessert, M. J. et al. Foot pressure distribution during walking in young and old adults. *BMC Geriatr.* **5**, 8 (2005).
39. Dickey, M. D. Emerging applications of liquid metals featuring surface oxides. *ACS Appl. Mater. Interfaces* 6, 18369–18379 (2014).
40. Terryn, S., Brancart, J., Lefeber, D., Van Assche, G. & Vanderborght, B. Self-healing soft pneumatic robots. *Sci. Robot.* **2**, eaan4268 (2017).
41. Shepherd, R. F., Stokes, A. A., Nunes, R. & Whitesides, G. M. Soft machines that are resistant to puncture and that self seal. *Adv. Mater.* **25**, 6709–6713 (2013).

Acknowledgements

The authors acknowledge support from the NASA Early Career Faculty Award (NNX14AO49G; Research Collaborator: B. Bluethmann) and AFOSR Multidisciplinary University Research Initiative (FA9550-18-1-0566; Program Manager: K. Goretta). M.D.B. also acknowledges support from Iowa State University start up funds. Sensor and mechanical characterization was performed on equipment supported through an Office of Naval Research (ONR) Defense University Research Instrumentation Program (DURIP) (N00014140778; Bioinspired Autonomous Systems; Program Manager: T. McKenna).

Author contributions

E.J.M., M.D.B., X.H. and C.M. designed the research; E.J.M., M.D.B. and X.H. performed the research; E.J.M., M.D.B., X.H. and C.M. analysed the data; E.J.M., M.D.B. and C.M. wrote the paper.

Competing interests

The authors declare no competing interests.

Additional information

Supplementary information is available for this paper at https://doi.org/10.1038/s41563-018-0084-7.

Reprints and permissions information is available at www.nature.com/reprints.

Correspondence and requests for materials should be addressed to C.M.

Publisher's note: Springer Nature remains neutral with regard to jurisdictional claims in published maps and institutional affiliations.

Methods

Fabrication. Polydimethylsiloxane (PDMS; Sylgard 184, Dow Corning) was prepared at a 5:1 oligomer/curing agent ratio using an AR-100 THINKY planetary centrifugal mixer (mixing: 1 min, defoaming: 1 min). Gallium and indium were purchased from Solution Materials, LLC and combined at 75% Ga, 25% In by weight to produce EGaIn. EGaIn will form an insulating ~0.5–3 nm oxide skin in the presence of oxygen[42,43]. The LMEE was fabricated by combining PDMS and EGaIn at LM loadings $\phi = 20$, 30, 40 and 50%, which corresponds to an LM-to-elastomer mass fraction of 1.61:1, 2.76:1, 4.30:1 and 6.44:1. The PDMS prepolymer and EGaIn were mixed until an emulsion was formed and no large droplets of EGaIn were visually present. The emulsion was then further mixed using a planetary mixer (mixing: 1 min), forming a polydisperse suspension of EGaIn microdroplets dispersed in the silicone elastomer matrix. Additional surfactants are not used as the oxide skin is sufficient as a dispersing and stabilizing agent for the droplets due to the affinity for both the silicone matrix and LM droplet[10]. After mixing, the composite could be cast or moulded and subsequently cured. For all materials presented, stencil lithography was used to pattern both bulk sheet and selectively patterned demonstrations (Blazer Orange Laser Mask, IKONICS Imaging), unless otherwise noted. First, a 300 µm layer of PDMS was cast on a polyethylene substrate and cured at 100 °C for 30 min using a thin-film applicator (ZUA 2000, Zehntner). The substrate was allowed to cool and a 550 µm layer of LMEE was cast on top of the PDMS layer using a stencil mask, the mask was removed and the layer was cured at 100 °C for 1 h. LM loading of $\phi = 50\%$ was used for all experiments unless otherwise noted. In practice, a 2D plotter is used to create the circuit on the exposed composite and then the circuit is sealed in insulating rubber (Sylgard 184, Dow Corning; cured at 100 °C for 30 min) to prevent further trace formation.

Material activation. The material was activated using a 2D plotter and scoring stylus by applying local pressure (Cricut Explore, Cricut). The scoring stylus was clamped in the cutting holder approximately 5.6 mm from the base (Supplementary Fig. 10). First, the material was adhered to the standard grip cutting mat, a custom tool (pressure: 150, passes: 5) was used to write the pattern, and the 2D plotter was operated as described in the user manual (see Supplementary Movie 1 for visual demonstration of activation). After activation, any LM residue on the surface was cleaned using a cotton tip applicator with isopropyl alcohol. To experimentally determine the minimum trace spacing, two parallel traces were drawn that were 100 mm in length to ensure sufficient overlap. Centre-to-centre trace spacings from 1 mm to 3 mm in 250 µm increments were tested. The resistance between the traces was measured using a multimeter (TOL-12967, SparkFun) to determine whether unintended activation had occurred between the closely neighbouring traces. Five samples for each spacing were tested to determine the minimum trace spacing. Additional details about the inadvertent activation are included in the Supplementary Information, including normal pressure activation, repeated compressive loading, shear activation and bending activation.

Electronic counter demonstration. A microcontroller (ATmega32u4, Atmel) was used to send serial commands through a four-wire interface to a seven-segment clock display with a serial interface (Adafruit). A section of the four-wire interface was replaced by the LM–elastomer composite to demonstrate the self-healing capabilities. The LMEE was prepared as described in the Fabrication section and the composite was activated as described in the Material activation section. The clock was updated every second.

Mechanical and electrical characterization. Samples were prepared in a dogbone geometry (Die A, ASTM D412A) and tested on a materials testing machine (5969, Instron) at a strain rate of 100 mm min^{-1}, unless otherwise noted. After sample fabrication (see the Fabrication section) and activation (see the Material activation section), the samples were glued (Sil-Poxy, Smooth-On) to 6-mm-thick acrylic grips and allowed to cure overnight, with the electrical contact outside the clamping area to reduce possible artefacts. For mechanical characterization, 1-mm-thick samples were moulded ($\phi = 0\%$, 50%). The samples were placed on a flat surface overnight at room temperature and post cured in a 100 °C oven for 1 h. For extended characterization, two traces were drawn down the centre of the dogbone as shown in Supplementary Fig. 5a. The sample was tested at an extension rate of 150 mm sec^{-1} using an orbital jigsaw (Black and Decker BDEJS600C) as previously described[2,44]. For electro-mechanical characterization, a single trace was drawn down the centre of the dogbone. For the resistance versus length and electro-mechanical coupling experiments, the resistance of the trace was measured using a micro-ohm meter (34420A, HP) with a four-point probe. The external analog data from the materials testing machine (2310–907, Instron) were collected at a rate of 1 kHz using an USB DAQ (USB-6002, NI). The data were collected using the serial interface (MATLAB, 2016a). For all electrical measurements, the electrical contact was scored using a razor blade and additional EGaIn was added to reduce the contact resistance.

IV curves. A Keithley 2460 SourceMeter with a four-point probe was used to generate current–voltage curves. A voltage of 1 V was sourced and the current was measured for $\phi = 20$–50% samples and a $\phi = 50\%$ sample was also evaluated by sourcing 5 A and measuring the voltage for a trace length of 45 mm. The relative change in temperature was calculated ($\Delta T = \Delta\rho/\alpha\rho_0$) using the temperature coefficient for gallium ($\alpha = 0.004$), an effective trace width ($w = 500$ µm) and thickness ($t = 550$ µm), trace length of 45 mm and electrical resistivity at room temperature ($\rho_0 = RA/\ell = (1.51)(2.75 \times 10^{-7})/(0.045) = 9.23 \times 10^{-6}\,\Omega$ m, where R, A and ℓ are the trace resistance, cross-sectional area and length, respectively).

Volumetric conductivity. The volumetric conductivity ($\sigma = \ell / RA$) for $\phi = 50\%$ was calculated using an effective trace width ($w = 500$ µm) and thickness ($t = 550$ µm; see Supplementary Fig. 3 for representative sample dimensions). The ℓ / R relationship was calculated by fitting a linear line with the y intercept equal to zero to the $\phi = 50\%$ data shown in Fig. 2a.

Self-healing characterization. The samples were prepared as described in the Fabrication section. The change in resistance was measured using a voltage divider with a 560 Ω resistor. The change in voltage across the LMEE was monitored using an USB DAQ (USB-6002, NI) and the data were collected at 50 kHz using a desktop computer (MATLAB, 2016a). The data were filtered using a low-pass filter.

Soft robot fabrication. The limbs of the soft quadruped use a SMA wire (0.3 mm diameter, Dynalloy) embedded in thermal tape (H48-2, T-Global). The SMA wire is bent into a U-shape with sharp corners (width = 13 mm, length = 55 mm) and bonded to thermal tape (length = 55 mm, width = 22 mm, thickness = 0.5 mm) using a thin layer (200 µm) of partially cured silicone elastomer (Ecoflex 00-30, Smooth-On; 7 min at 50 °C). A second layer of silicone elastomer (400 µm) is applied to the stack and partially cured (7 min at 50 °C). In parallel, a 200 µm layer of silicone elastomer is partially cured on pre-stretched ($\lambda = 1.5$) thermal tape (length = 70 mm, width = 60 mm, thickness = 0.5 mm). After curing, the layers are clamped together with binder clips and fully cured at 50 °C for 10 min. The excess material is cut off along the outline of the unstretched thermal tape layer. The soft actuator layer stack is shown in Supplementary Fig. 11a.

Each of the limbs is glued (All-Purpose Krazy Glue) to an acrylic frame. Non-insulated wire ferrules are crimped to the ends of the SMA wire and soldered to ring terminals that are mechanically fixed to the acrylic frame using bolt and nut fasteners. The fasteners provide an electrical connection to the LMEE sheet similar to a via in a printed circuit board. The LMEE sheet is placed over the bolts and nuts are used as a clamp to mechanically and electrically connect the LMEE sheet to the acrylic frame, SMA actuators and control board. A cross-section view of the electrical and mechanical connection and general dimensions of the acrylic frame are shown in Supplementary Fig. 11b,c. Additional details are included in the Supplementary Information.

Data availability. The data that support the findings of this study are available upon request from the corresponding author.

References

42. Cademartiri, L. et al. Electrical resistance of Ag^{TS}–$S(CH_2)_{n-1}CH_3$//Ga_2O_3/EGaIn tunneling junctions. *J. Phys. Chem. C* **116**, 10848–10860 (2012).
43. Regan, M. et al. X-ray study of the oxidation of liquid-gallium surfaces. *Phys. Rev. B* **55**, 10786 (1997).
44. Pendergraph, S. A., Bartlett, M. D., Carter, K. R. & Crosby, A. J. Opportunities with fabric composites as unique flexible substrates. *ACS Appl. Mater. Interfaces* **4**, 6640–6645 (2012).